Motion Planning in Stereotaxic Radiosurgery

Achim Schweikard, John R. Adler, and Jean-Claude Latombe

Abstract—**Stereotaxic radiosurgery is a procedure that uses a beam of radiation as an ablative surgical instrument to destroy brain tumors (or more generally, brain lesions). The beam is produced by a linear accelerator that is moved by a mechanical gantry. Radiation is concentrated by crossfiring at the tumor from multiple directions, to reduce the amount of energy deposited in healthy tissues. Because access to and exit from the tumor is obstructed along some directions by critical structures (e.g., brain stem, optic nerves), planning the path of the beam is often difficult and time-consuming. This paper describes a computer-based planner developed to interactively assist the surgeon generate a satisfactory treatment, given the spatial distribution of the brain tissues obtained with medical imaging. This planner has been experimented on using 11 cases previously processed at the Stanford Medical Center. A dosimetric comparison with the manually generated plans for these cases was carried out. Although still limited, results indicate that automatic planning can significantly improve energy deposition. It can also shorten the overall treatment, hence reducing the patient's pain and allowing the radiosurgery equipment to be used for more patients. Stereotaxic radiosurgery is an example of so-called "bloodless surgery." Computer-based planning techniques are expected to facilitate further development of this safer, less painful, and more cost effective type of surgery.**

I. Introduction and Background

STEREOTAXIC radiosurgery is a precision procedure that uses an intense focused beam of radiation as an ablative surgical instrument. The treatment uses the spatial information provided by computerized tomography (CT) and magnetic resonance imaging (MRI) for targeting. Several leading medical schools worldwide have recently reported dramatic success with this technique in the treatment of brain tumors [2] and malformations [3]. In addition to being safer than conventional operations, this procedure is much less expensive.

Although radiosurgical procedures have been utilized in a limited way for over 20 years, it was only with the advent of CT and MRI that many new applications for radiosurgery were developed. By coupling stereotaxic precision localization with a sharply collimated beam, specialized instrumentation makes it possible to target a biologically ablative dose of ionizing radiation to a well-circumscribed brain lesion. With an accuracy approaching 1 mm, a very large "necrosing" dose of radiation (1 000 to 5 000 rad) is delivered at a single sitting. Radiosurgical treatment often supplants a major operation and is typically done on an outpatient basis. It allows treatment for many brain lesions which are typically inoperable.

Presently there are three types of radiosurgical techniques that are distinguished by radiation source:

- Static beam of heavy charged-particles (protons or helium ions) generated by a synchrocyclotron [14].
- Static array of 201 Co^{60} sources (Gamma-knife) [18].
- Photon beam produced by a standard medical linear accelerator moved by a gantry [12].

These techniques are discussed and compared in various publications. For example, see [23]. Radiophysical and clinical studies suggest that under most circumstances the three techniques are comparable. However, due to its greater flexibility and relatively low cost, linear accelerator techniques (LINAC) are the most widespread. During treatment, the accelerator moves around the patient's head along a predefined path, so that the radiation is concentrated by crossfiring at a target volume (often a tumor) from multiple directions and the amount of energy deposited in normal tissues is relatively small.

The overall stereotaxic radiosurgery treatment consists of the following steps:

1) A metal frame, called a stereotaxic frame, is attached under local anesthesia to the patient's skull using screws or pins. The position of the frame with respect to the jointed mechanism is adjusted by means of a micrometric system. Hence, it is known with high precision.
2) CT and MR images are obtained and analyzed with the frame attached. The locations of both the tumor and the critical structures are determined with respect to the frame.
3) A path for the radiation beam is planned based on this spatial information and the intensity of the beam along this path is selected. The dose distribution corresponding to this path is computed by a dosimetry program. This program embeds a model of the fluence of the radiation beam through the brain tissues and integrates this fluence over time at every point of interest. The results are visualized on a graphic display. If the surgeon finds the distribution acceptable, the treatment proceeds to step 4); otherwise another path is generated.

Manuscript received September 14, 1992; revised February 15, 1993. This work was supported in part by the Sheikh Hassan M. Enamy Gift Fund.

A. Schweikard is with both the Department of Computer Science and the Department of Neurosurgery, Stanford University, Stanford, CA 94305.

J. R. Adler is with the Department of Neurosurgery, School of Medicine, Stanford University, Stanford, CA 94305.

J.-C. Latombe is with the Robotics Laboratory, Department of Computer Science, Stanford University, Stanford, CA 94305.

IEEE Log Number 9212596.

4) The gantry moves the activated beam along the path accepted by the surgeon.

This procedure is quite long; it takes on the order of 30 min, 1–2 h, 2–3 h, and 1–2 h for steps 1), 2), 3), and 4), respectively.[1] The patient is conscious throughout all steps, and the stereotaxic frame, which remains attached to his/her head (since the correspondence between the images and the gantry must be maintained), is painful. Shortening the procedure would reduce the patient's discomfort. Furthermore, it could save time for the surgeon and allow the treatment of more patients with the same equipment. In this context, various computer techniques can be applied. In particular, in step 2), image interpretation techniques can be used to automatically locate regions of interest. Several such techniques have been reported in the literature (e.g., see [6], [17]). Meanwhile, in step 3), planning techniques could be used to generate appropriate beam motions. The latter objective is the topic of this paper.

Many of the brain tumors that are considered inoperable involve the skull base and are adjacent to critical structures such as the optic nerve and chiasm, carotid artery, and brain stem. Although radiosurgery has proven to be a valuable and often times curative treatment for these lesions, their close proximity to such important and extremely radiation-sensitive areas is problematic. Since damage of these structures can result in such severe side effects as a paralysis or blindness, the path of the beam must be selected so as to minimally irradiate them. Finding the best trajectory for a radiation beam is further complicated by the typically irregular shape such tumors assume. Despite the complexity of treatment planning it is currently done manually. Given that the problem is largely one of geometric reasoning, it would seem reasonable that it might be done better and faster by computer. It is this hypothesis that is investigated in this paper.

The planning problem considered in this paper has been recently termed the "inverse dosimetry problem" [13], [1]. Given a spatial map of the brain and a treatment plan, the goal of the direct dosimetry problem is to compute energy deposition in brain tissues. This problem is currently solved by dosimetry programs embedding models of the fluence of the radiation beam as it travels through tissues. Meanwhile, the inverse problem is how to deliver a specific dose of radiation to a target volume without, at the same time, irradiating healthy tissue beyond tolerance [1]. Previous research sought to find a mathematical solution of this problem by solving an integral equation: given the desired dose distribution and the equation expressing the dose received at any one point as the integral over time of the fluence of the radiation beam, solve this integral for the fluence of the beam throughout the treatment. The approach is promising and progress has been reported over the last few years, [1] [4], [5], [7], [8]. However, existing results still only apply to simple dose distributions in two dimensions. It seems that it will be extremely difficult to handle realistic three-dimensional dose distributions. Furthermore, the integral equation does not take some important parameters into account. For example, treatment plans may be generated that are too complicated to execute, or even not feasible, due to mechanical constraints in the system moving the radiation beam.

Our approach to radiosurgical planning is different. It derives from geometric computation techniques developed for robot motion planning [15]. We treat the critical brain structures as "obstacles" that the radiation beam is not allowed to traverse. Hence, we represent them as volumes obstructing beam access to and exit from the tumor. Our planner computes an explicit representation of all the allowed motions of the beam when it crossfires at the tumor. From this representation, it extracts connected arcs of maximal length, which makes it possible for the beam to strike the tumor from many different directions and thus reduce the dose received by healthy tissues (other than the critical structures). These arcs define the path of the beam generated by the planner. The intensity of the beam along this path is computed in a straightforward manner by assuming no attenuation of the fluence of the beam when it travels through brain tissues. Our planner could likely be improved by using a better model of the fluence of the beam and applying inverse dosimetry techniques such as those evoked in the previous paragraph to select the intensity of the beam along every computed arc.

In its current form, our planner solves a purely geometric problem. The user (typically, the surgeon) defines interactively the number of arcs to be computed, as well as parameters constraining these arcs (e.g., the minimal length of each arc, the minimal angle between the planes containing any two arcs). Hence, our planner is mainly a computational tool to assist the surgeon in exploring several possible treatment plans. It guarantees that the arcs it generates satisfy the constraints defined by the input parameters, and it is complete (that is, it always find such arcs if they exist). However, these properties are not sufficient to guarantee the optimality of the selected treatment. In fact, since it seems impossible to propose a comprehensive optimality criterion taking all parameters into account (desired dose distribution, duration of treatment, patient's medical history), we feel that providing the surgeon with an interactive tool to explore the range of possible treatment plans is currently the most suitable way to proceed.

Our planner has been developed for a specific LINAC system based on Brown–Roberts–Wells stereotaxic localization, which is available at the Stanford Medical Center (see Section II). We present preliminary experimental results obtained with this planner on two recorded cases and compare these results with the manually planned treatments that were actually performed. Although still preliminary, these results and similar ones obtained on nine other recorded cases indicate that motion planning software can both significantly reduce energy deposition in

[1]These durations and other information are given here to help the nonspecialist reader apprehend the motivation for the work described in this paper.

critical tissues and dramatically shorten the duration of step 3), for complex cases.

Very different image-guided robotics systems have been developed for other types of surgical applications [16], [21]. The system in [16] is used for inserting electrodes or radioactive seeds into a patient's brain with high accuracy; the electrode or seed is moved to an appropriate entry position by a six-degrees-of-freedom robot and then moved into its final placement in the brain by the surgeon. A robotics system designed to create femoral cavities that are precisely shaped and positioned for inserting uncemented prostheses is described in [21]. Motion planning techniques could also be beneficial to the development of these systems. However, the planning issues they raise are different from those of radiosurgery.

The rest of the paper is organized as follows. Section II presents the kinematics of our LINAC system and the standard treatment with this equipment. Sections III–V describe the geometric methods used in our planner. Sections VI and VII discuss the implementation of the planner and experimental results.

II. LINAC System

Although there are several LINAC-based systems [23], one of the most frequently used devices is based on the Brown–Roberts–Wells stereotaxic localization [20], [25]. The experimental work reported in this paper has been carried out with such a system, which is described here. In the rest of the paper, this system will be referred to as the LINAC system.

The radiosurgery equipment used in our work is depicted in Fig. 1. It consists of a floor stand (couch) with four joints and a gantry with a revolute joint moving a 6-MeV photon source generating a circular beam. The position of the floor stand can be adjusted with three prismatic joints. Its orientation in the horizontal plane is set by a revolute joint about the axis designated by $\boldsymbol{T}$ in Fig. 1. The linear accelerator can be moved by rotating the gantry about the axis denoted by $\boldsymbol{G}$. The beam central axis is denoted by $\boldsymbol{C}$. The three axes $\boldsymbol{T}$, $\boldsymbol{G}$, and $\boldsymbol{C}$ always intersect in one point. While the accelerator is rotated, the floor stand joints remain fixed, so that the beam can only span vertical angular sectors. The radius of the beam generated by the accelerator can be adjusted by inserting a lead collimator into the accelerator. The beam can be turned on and off during the motion.

The standard treatment using this equipment is the following. Assume first that the tumor is approximated[2] as a ball $\mathfrak{I}$. The prismatic joints in the floor stand are adjusted such that the intersection point of $\boldsymbol{T}$, $\boldsymbol{G}$, and $\boldsymbol{C}$ coincides with the center of $\mathfrak{I}$. The beam radius is set to the radius of $\mathfrak{I}$. The revolute joint of the floor stand (axis $\boldsymbol{T}$) is set to a fixed angular position α_1. In this position the gantry is moved around $\boldsymbol{G}$ between two orientations β_1 and β_1',

[2]Approximating a tumor by a target ball (or a set of balls) is a delicate issue that will be briefly addressed in Section VI.

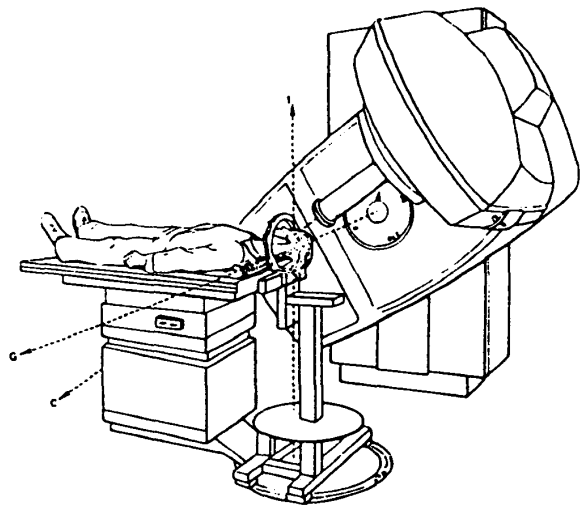

Fig. 1. Schematic of radiosurgery equipment [25].

while the beam is activated. In this way the beam spans a vertical angular sector whose apex is the center of $\mathfrak{I}$. Furthermore, throughout the motion, $\mathfrak{I}$ is inside the beam. The floor stand revolute joint is then set to a new angular position α_2 and a second arc (β_2, β_2') is generated by moving the gantry, and so on. The standard motion procedure described in [20] consists of four such arcs. The angle between any two planes containing these arcs should be large enough so that the volumes swept by the beam when it moves along the various arcs have small intersection outside $\mathfrak{I}$. It is thus ensured that the dose inside $\mathfrak{I}$ largely exceeds the dose absorbed by surrounding tissues. Energy deposition can be computed by a standard dosimetry program that is currently in clinical use at Stanford. If this computation shows too large a dose to critical regions, the 4-arc path is modified by changing the floor stand angles, the gantry motion ranges, and/or the beam intensity along each arc.

When the tumor is not spherical, it is approximated as a collection of nonintersecting spheres. Each sphere is treated independently as described above.

The planner presented below directly applies to this system and generates standard 4-arc paths. However, it has the potential to be more general. In particular, with the same system kinematics, it can generate paths with an arbitrary number of arcs, which allows a better distribution of energy in the brain, especially when the tumor and critical structures are adjacent to one another. Extensions (not described in this paper) would also allow the planner to deal with a less constrained mechanical gantry. This is important since the study reported in [22], [23] shows that better energy deposition can be achieved by using a system with more versatile kinematics. In fact, we plan to soon replace our current gantry by a robot arm allowing arbitrary 6-degrees-of-freedom motions of the linear accelerator and we plan to extend our planner to this new system (see Section VIII).

III. Geometry of the Beam Configuration Space

Our planning approach is mainly geometric. We explicitly represent the set of all orientations of the beam where it crossfires at the tumor without intersecting any of the critical regions in the brain. From this representation we extract a set of circular arcs defining a possible path of the beam. In this section we show how a set of valid orientations of the beam can be generated. Arc computation will be described in the next section.

A. Beam Configuration Space

Let us assume that the tumor is modeled as a target ball of radius r centered at the coordinate origin O. A *configuration* of the radiation beam is defined as the orientation of its central axis **C** when this axis goes through O. In the following, we assume that the energy distribution along the beam is constant; hence, any two opposite orientations of the beam are equivalent. We can then represent a beam configuration by the two antipodal points where its central axis intersects the unit sphere S^2 centered at O. The set of all beam configurations, i.e., the beam's *configuration space*, is thus represented as the sphere S^2 with antipodal points identified.

The kinematics of our LINAC system constrains the beam configuration to move along arcs of great circles of S^2 contained in vertical planes. A path of the accelerator is thus defined as a series of such arcs.

Our planning techniques treat critical regions as obstacles that should not be intersected by the beam. This leads to precomputing the map of each critical region into S^2 as a set of forbidden configurations called the *C-obstacles*. The complement of the C-obstacles in S^2 is called the *free space*.

B. C-Obstacles

Let C_i, $i = 1, \cdots, m$, denote the critical regions of the brain. Each region C_i maps into S^2 as follows.

We grow C_i isotropically by the radius r of the target ball (i.e., the radius of the beam); this yields a grown region C_i'. Intuitively, C_i' is obtained by moving a ball of diameter r to all placements where it is in contact with C_i without overlapping it; C_i' is equal to C_i enlarged by the volume swept out by the ball. More formally, we have

$$C_i' = C_i \oplus B_r = \{c + b \mid c \in C_i, b \in B_r\},$$

where B_r is the ball of radius r centered at the coordinate origin O and $\oplus$ denotes the Minkowski set sum.

Hence, if the beam central axis does not cross the enlarged region C_i', then the beam does not intersect C_i. The central projection of C_i' from O into S^2 gives the C-obstacle corresponding to C_i. Note that each C-obstacle consists of two antipodal regions.

C. Computation of Free Space

The following simple technique can be used to compute an approximation of free space.

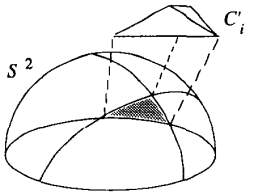

Fig. 2. Construction of free space.

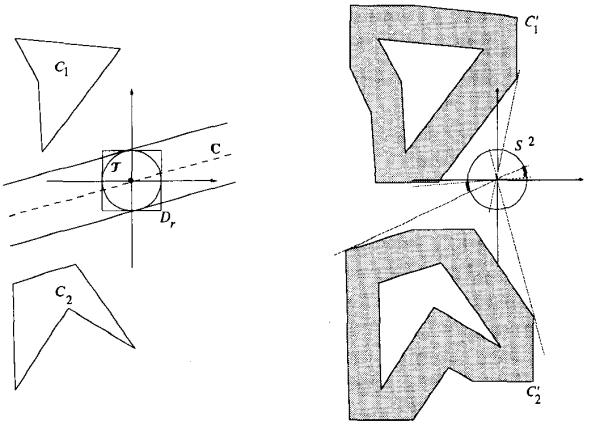

Fig. 3. Computation of free configurations in a two-dimensional example.

Let C_i, $i = 1, \cdots, m$, be polyhedra approximating the critical regions and D_r be a polyhedron bounding the ball B_r. (In our implementation, D_r is simply a cube of edge length $2r$ centered at O.) We construct each C_i' as $C_i \oplus D_r$, rather than $C_i \oplus B_r$. C_i' is then a polyhedron whose computation is studied in [19], [10]. This approximation yields a particularly simple projection of C_i' into S^2. Indeed, each edge E of C_i' maps to an arc of great circle that is the intersection of the plane containing O and E with S^2. The set of edges of all grown regions C_i' thus determines a collection of great circles which partition S^2 into an arrangement of regions (see Fig. 2). The free space is the union of a subset of these regions.

Let n be the total number of vertices of the polyhedra $C_1, \cdots, C_m$. Let the number of vertices of the polyhedron D_r be small enough to be considered $O(1)$. The grown regions C_i' can be computed in $O(n)$ time using the algorithm described in [10]. They have a total of $O(n)$ vertices and thus yield $O(n)$ great circles in S^2 forming an arrangement of $O(n^2)$ regions. This arrangement can be computed in $O(n^2)$ time by a topological sweep algorithm [9].

Example: Free-space computation is illustrated in Fig. 3 with a simple two-dimensional example. (The beam configuration space is then the unit circle S^1.) In Fig. 3(a), C_1 and C_2 are polygons approximating critical regions, **C** is the beam central axis at some arbitrary free configuration of the beam, and D_r is the bounding square containing the target disc $\mathfrak{I}$. In Fig. 3(b), C_1' and C_2' are the grown regions corresponding to C_1 and C_2. Each grown region

is projected into S^1 as two antipodal arcs (the C-obstacles). The complement of these arcs, i.e., the two antipodal arcs shown in bold lines, represents free space.

In the following, we assume that C-obstacles and free space have been computed using the above approximation. They are therefore bounded by arcs of great circles.

IV. Computation of Vertical Free Arcs

In this section we show how free arcs defining the path of the LINAC system can be extracted from the free space computed as above. We first keep our presentation independent from the kinematic limitations of this system (Section IV-A). We then explicitly deal with these limitations by focusing on the generation of free vertical arcs (Sections IV-B and IV-C).

A. Characterization of Great Circles

Let g be any great circle of S^2. We can represent g by two antipodal points of a sphere DS^2, the *dual sphere* of S^2, defined as the extremities of the two opposite unit vectors erected at O and normal to the plane containing g.

Let e be an edge (arc of great circle) of a C-obstacle and u and v be its endpoints. Let $G(u)$ be the set of all great circles of S^2 containing u. This set maps into DS^2 as a great circle $n(u)$. In the same way the great circles of S^2 containing v map to a great circle $n(v)$ of DS^2. The two circles $n(u)$ and $n(v)$ partition DS^2 into four regions. Two of these regions represent the great circles in S^2 that intersect the arc e. The other two regions represent the great circles in S^2 that do not intersect e.

Consider the C-obstacle edges in S^2. The set of great circles corresponding to the endpoints of these edges partition DS^2 into an arrangement A of regions. Let R be any such open region of dimension 2, and let p be any point in R. The great circle of S^2 corresponding to p intersects a possibly empty set of C-obstacle edges. By construction of the great circles forming A, when p moves in R, this set remains constant. We denote it by $\sigma(R)$. We called R a *regular region* of DS^2 and $\sigma(R)$ the *characteristic set* of R.

The arrangement A is created by $O(n)$ great circles. It contains $O(n^2)$ regions and can be computed in $O(n^2)$ time (as above, n is the total number of vertices of the critical regions). The characteristic set of any region in A can be computed in $O(n)$ time. By noticing that the characteristic set undergoes minor changes between two adjacent regular regions, which can be computed in constant time, it is possible to generate all characteristic sets in $O(n^2)$ time.

However, the LINAC system can only move the beam source along arcs of vertical great circles. Although the computation of A and the characteristic sets can be useful for a more versatile mechanical system, it is too general here.

B. Free Vertical Great Circles

Vertical great circles of S^2 are represented by points of the horizontal circle H of DS^2. The intersection points of H with the circles of the arrangement A decompose H into arcs. Let $L = (s_1, s_2, \cdots)$ be the sorted list of these arcs. All vertical great circles represented by points in the same arc s_i intersect the same C-obstacle edges (possibly none). Let $r(s_i)$ denote the number of C-obstacle edges intersected by the great circle of S^2 represented by any point of s_i; $r(s_i)$ is equal to the size of the characteristic set of the region of A containing s_i (although it can be computed more directly). If $r(s_i) = 0$, then all points in s_i represent free great circles of S^2. By scanning the list L of arcs of H, we can identify all arcs s where $r(s)$ reaches 0 and report the sublist of these arcs, which represents all free vertical great circles of S^2.

As mentioned above, this computation does not require the precomputation of the characteristic sets of the regions of A. The intersections of H with the circles generating A can be computed in $O(n)$ time. The sorted list L is thus produced in $O(n \log n)$ time. The number $r(s_1)$ can be computed directly in $O(n)$ time. The arcs s_1 and s_2 are separated by a point where h intersects a great circle of A. By analyzing this intersection, one can compute $r(s_2)$ from $r(s_1)$ in constant time. In the same way, each new number $r(s_i)$ can be computed in constant time from $r(s_{i-1})$. Hence, the list of arcs s verifying $r(s) = 0$ is generated in $O(n \log n)$ time.

C. Free Vertical Arcs of Given Length

In many cases, however, there are no free vertical great circles or the existing ones do not have sufficient angular distance between them (see Section II). Therefore, it may be more interesting to compute vertical great circles in which free arcs have accumulated length greater than some specified value K. When the accelerator is moved along such a circle, the beam must alternately be turned on and off.

The vertices of the free space in S^2 map to a collection of great circles of DS^2. These circles partition H into a list $L' = (s'_1, s'_2, \cdots)$ of arcs ($L \subseteq L'$). Consider any arc s'_i in this list. All vertical great circles of S^2 represented by the points of s'_i intersect the same C-obstacle edges *in the same order*. We decompose every arc s'_i into subarcs such that when a point p varies from one extremity of any subarc to the other, the total length of free arcs in the great circle of S^2 represented by p increases or decreases monotonically. Each subarc of H thus contains at most one connected segment representing great circles containing free arcs with total length greater than the given threshold K.

The number of segments thus extracted from H is polynomial in n. The computation also requires polynomial time. It involves finding the zeros of polynomial equations. We will not discuss this issue here, since the implemented planner makes use of an approximate technique based on discretizing H (see Section VI).

One may alternatively consider great circles containing a connected free arc whose length is greater than some value. The computation of such great circles can be done with a technique very similar to the above.

V. Path Planning

A path of the LINAC system consists of a series of arcs (connected or not) contained in different vertical great circles. We consider the path planning problem defined by three parameters: the radius r of the target ball approximating the tumor, the number k of great circles, the minimal cumulative length K of the free arcs in each great circle, and the minimal angle ω between the planes of any two great circles. The planner used the value of r to compute free space. Then it generates a path as follows.

We give an arbitrary orientation to the horizontal great circle H of DS^2. Let $(s_1^\kappa, s_2^\kappa, \cdots)$ be the sorted list of the arcs of H representing the vertical great circles of S^2 whose free arcs have a total length greater than K. We must find a series of k points $p_1, \cdots, p_k$ in these arcs such that the angle $\omega(p_i, p_j)$ between the vertical planes containing the great circles represented by any two points p_i and p_j is larger than ω. (Note that $\omega(p_i, p_j)$ is equal to the angular distance between p_i and p_j in H.)

Assume that points p_i have been computed. If none coincides with an endpoint of arc s_j^κ, then we can move all the points p_i simultaneously, in the direction opposite to that of H, until one reaches an endpoint of an arc s_j^κ. Therefore, to compute the points p_i, we can assume that one point coincides with the first endpoint of an arc s_j^κ (the arc being oriented as H).

We begin by placing the point p_1 at the first endpoint of an arbitrarily selected arc s_{j1}^κ. We then move in the direction of D and place p_2 within an arc s_{j2}^κ (possibly, equal to s_{j1}^κ), such that the angular distance between p_1 and p_2 is minimal, but larger than ω. After placing p_1 and p_2, the remaining points are positioned in the same way. Whenever a new point is positioned, it is also verified that its angular distance to p_1 is greater than or equal to ω. If no appropriate placement is found for any point p_2 through p_k, p_1 is selected at the first endpoint of another arc and the construction is repeated.

If the planner terminates successfully, it provides a set of k great circles satisfying the input constraints, along with the free arcs in each great circle. If it fails to find a path, one can modify the constraints, i.e., the values of r, k, K, and ω. It is easy to show that the planner is complete, that is, if there exist k vertical great circles, each containing free arcs of total length K (or more), whose planes make angles greater than or equal to ω, it is guaranteed to return such circles; otherwise it returns failure.

Assume that the arcs s_j^κ in H have already been computed. Let q be the number of these arcs. For a given position of p_1, the placement of every point p_i takes $O(\log q)$ time. The placement of all points, if possible, thus takes $O(k \log q)$ time. In case of successive failures, the process is repeated up to q times, yielding a total planning time of $O(kq \log q)$. If $K = 2\pi$ (i.e., if we are only interested in great circles), then $q \in O(n)$. If $K < 2\pi$, then q has a higher-degree polynomial dependence on n.

Alternatively, a problem can be defined so that each great circle contains a connected free arc of length greater than or equal to K. The selection of the points p_i is done in the same way as above.

VI. Implementation

An interactive planner based on the techniques described above has been implemented to compute appropriate multiarc paths for our LINAC system. The software is written in C and runs on a Silicon Graphics workstation. The planner has been connected with dosimetry and imaging software already in use with the stereotaxic system at the Stanford Medical Center.

CT and MR images give the anatomy of the brain in parallel axial cross sections separated by 3 to 5 mm. The critical regions in each cross section are delineated by polygons. These polygons are then "thickened" by the distance between cross sections, thus yielding a polyhedral approximation of every critical region. Currently, the delineation operation in each cross section is done manually.

The planner is interactive. The user (typically, the surgeon) sets the parameters r, k, K, and ω. The planner generates a path made of multiple arcs satisfying the constraints entailed by these parameters, if such arcs exist. The dose distribution corresponding to this path is computed and visualized. The user can modify the input parameters iteratively to get different paths, hence different treatment plans.

The planning algorithm works as described in Section V, with the difference that the horizontal great circle H in DS^2 is discretized into N equidistant points (typically, $N = 128$). For every point p in the discretization of H, the planner computes the set of free arcs in the great circle of S^2 represented by p and the total length (or maximal length) of these arcs. This leads the planner to compute each arc s_j^κ as a list of points, instead of a continuous segment. The rest of the planner operates in the same way as above. The implemented planner is resolution-complete: if there exist arcs satisfying the input constraints, it is guaranteed to find them, provided that N be large enough. The value $N = 128$ used in our experiments led to satisfactory results.

The planner either returns a path (set of arcs) or indicates failure. If it returns a path, the dosimetry program is run and computes the energy deposition in the brain tissue that will result from the execution of this path. If the surgeon does not find this distribution acceptable, the planner is called back with different parameters (r, k, K, and/or ω). If the planner fails to return a path, it can also be called back with different parameters.

The planner incorporates several straightforward improvements. For example, when it finds a path, it can iteratively rotate the k vertical planes containing the planned arcs to maximize the minimal length of free arcs in each one. When it fails to find a path satisfying the constraints, it can find, by bisection, the maximal ω for which there is a path.

Currently, we assume in the planner that the fluence of the beam is constant throughout tissues and perfectly focused. (However, the dosimetry program used to evaluate plans incorporates a more sophisticated state-of-the-art model of the beam fluence.) The fluence is set by the planner to the same value along the k arcs, proportional to the inverse of the total length of these arcs. A potential improvement of the planner, which we have not explored yet, is to allow for a different beam intensity along each arc. This could be done by using results obtained with the inverse dosimetry problem (e.g., [1]). In fact, since the general form of this problem seems extremely complex, one could use our planner to generate a set of arcs defining a class of treatment plans and then inverse dosimetry techniques to select an optimal or quasi-optimal plan in this class.

An important issue not investigated, so far, is tumor representation. An almost spherical tumor can be well represented by a single target ball. But this ball is not necessarily the one that achieves the best geometrical match with the tumor. Actually, because the radiation beam is not perfectly focused and there is some dose fall-off in the vicinity of the target ball, it is often suitable to approximate the tumor by a smaller ball. When the shape of the tumor is more complicated, one may represent it by several balls; a distinct path can be generated for each ball. For the same reasons as above, these balls should be separated by some space. To eventually simplify the use of our planner and improve the generated treatment plan, a geometric method for approximating tumors by a given number of balls was implemented. This method is based on an algorithm described in [24] for finding the smallest sphere containing a set of points in space. However, this work is still not well developed and requires additional research. Ultimately, we see tumor representation an integral part of the planning problem.

VII. Experiments

In order to carry out a preliminary evaluation of the planner, we ran it on 11 cases that had previously been treated with the LINAC system at the Stanford Medical Center. In each case, the dose distribution for the treatment computed by the planner was compared to the distribution for the original treatment that had been generated manually. Comparison was done at a large number of critical points (only a subset of them are given below). Although a more global (volumetric) evaluation could be useful, we do not think that it would yield significantly different results. We report two representative cases below, taken from our 11 experimental cases.

To make comparison with manual planning realistic, the planner was run with $k = 4$ and an initial value of ω equal to the standard 45°. We also requested the planner to find great circles containing a connected free arc of length greater than some K. When the planner found a path, this path was automatically optimized as explained above. When the planner failed, ω was determined by bisection. In all cases, the planner took on the order of 1–2 min to generate a treatment (including C-obstacle computation).

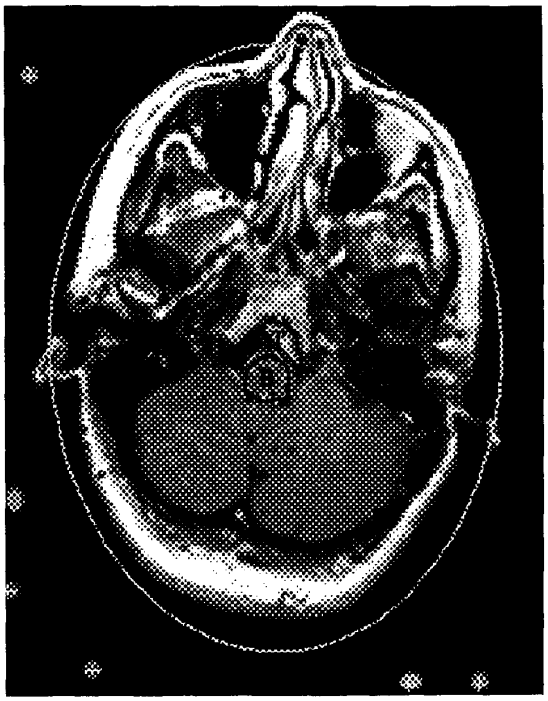

Fig. 4. Axial cross section of the brain in Case 1.

The planner was also used to generate paths with more than four vertical arcs. Interestingly, this usually led to relatively small dosimetric improvements. On the other hand, limited additional experiments have shown that in some cases the restriction to vertical arcs impairs dose distribution (see Section VIII).

Our experiments with tumors of complex shape (i.e., whose representation requires several target balls) have been very limited so far. Although encouraging, results are not significant yet. No such case is reported below.

A. Case 1

Fig. 4 shows the CT image of an axial cross section of the brain. A single critical region (brain stem) is delineated by a polygon B. The tumor is designated by T. Both the manually generated path and the computed path consist of four connected arcs in different planes. They were generated for a tumor approximated by one sphere of radius 10 mm.

Fig. 5 shows the energy deposition computed by the dosimetry program in four cross sections distant by 3 mm for the manually generated path. Fig. 6 shows the deposition computed for the path generated by the planner. In both figures, doses are shown as gray levels in steps of 200 centiGray (1 Gray = 1 j/kg).

Quantitative dose values are given in Table I for both plans, at the vertices of the brain stem B in five cross

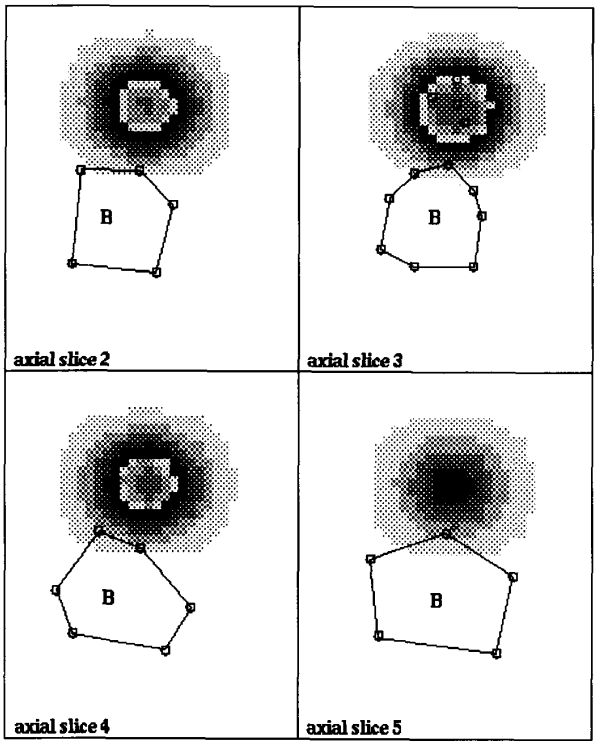

Fig. 5. Dose distribution for the manually planned treatment in Case 1.

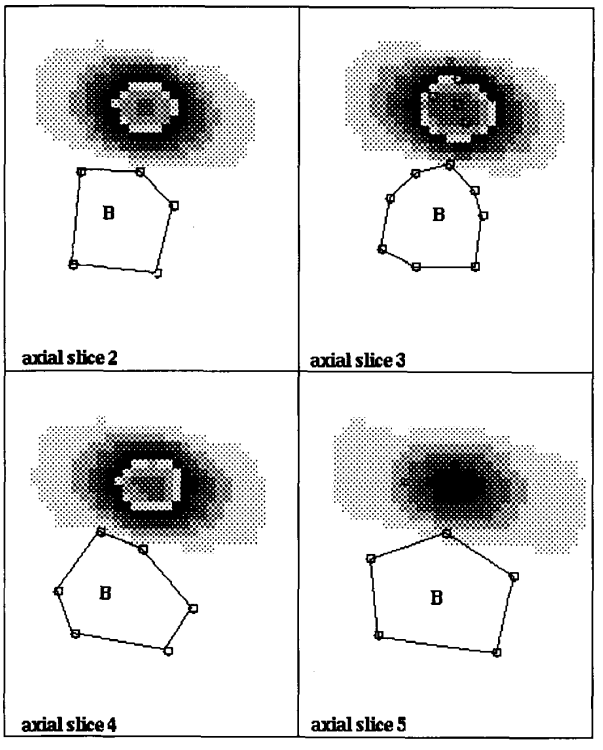

Fig. 6. Dose distribution for the automatically planned treatment in Case 1.

TABLE I
COMPARISON OF ENERGY DOSES IN THE BRAIN STEM (CASE 1)

	manually planned motion		computed motion	
BrStem.1.1	177.8	8.9	80.9	4.1
BrStem.1.2	76.7	3.8	10.8	0.5
BrStem.1.3	13.7	0.7	0.0	0.0
BrStem.1.4	14.5	0.7	0.0	0.0
BrStem.1.5	42.5	2.1	1.4	0.1
BrStem.2.1	161.0	8.0	23.9	1.2
BrStem.2.2	121.7	6.1	25.8	1.3
BrStem.2.3	60.7	3.0	1.6	0.1
BrStem.2.4	33.2	1.7	0.0	0.0
BrStem.2.5	32.6	1.6	0.0	0.0
BrStem.3.1	239.5	12.0	55.0	2.8
BrStem.3.2	60.3	3.0	0.5	0.0
BrStem.3.3	68.5	3.4	1.7	0.1
BrStem.3.4	37.0	1.9	0.0	0.0
BrStem.3.5	144.2	7.2	18.6	0.9
BrStem.3.6	90.9	4.5	6.0	0.3
BrStem.3.7	38.7	1.9	0.0	0.0
BrStem.3.8	38.5	1.9	0.0	0.0
BrStem.4.1	163.2	8.2	19.4	1.0
BrStem.4.2	242.6	12.1	106.6	5.4
BrStem.4.3	43.8	2.2	1.2	0.0
BrStem.4.4	30.6	1.5	0.0	0.0
BrStem.4.5	30.0	1.5	0.0	0.0
BrStem.4.6	40.6	2.0	0.3	0.0
BrStem.5.1	313.4	15.7	165.6	8.4
BrStem.5.2	88.2	4.4	50.2	2.5
BrStem.5.3	8.0	0.4	0.0	0.0
BrStem.5.4	11.1	0.6	0.0	0.0
BrStem.5.5	89.9	4.5	30.1	1.5
	(a)	(b)	(c)	(d)

sections. The first column contains point labels. The second and fourth columns show the dose values for the manually planned path and the computed path, respectively, in centiGray (cGy). The third and fifth columns show these values in percent of the dose deposited at the center of the sphere approximating the tumor. A nonzero dose is computed in some vertices of *B* for the automatically planned path, despite the fact that nowhere along this path the beam intersects *B*. In fact, the beam is not perfectly focused and the dose close to the theoretical cylinder modeling the beam is not exactly null. The dosimetry program makes use of a model of the beam that takes this into account. If the surgeon considers that the dose received by some areas in the critical structures is too high, he/she can rerun the planner with a smaller target ball.

An elevated relative dose is obtained for vertices close to the tumor, mainly at points BrStem.5.1, BrStem.4.2, and BrStem.3.1. Table I shows that the dose at these points is reduced in the computed path by 46, 55, and 76 percent, respectively, relative to the manually planned path. The table shows a substantial dose reduction ratio at all other vertices, but these reductions are less critical since the doses for the manually generated paths are significantly lower.

B. Case 2

Fig. 7 shows the CT image of an axial cross section of the brain for Case 2. Two critical regions *B* (brain stem) and *OC* (optic nerve and chiasm) are delineated by polygons. The tumor is designated by *T*. Again both the manually generated path and the automatically computed path

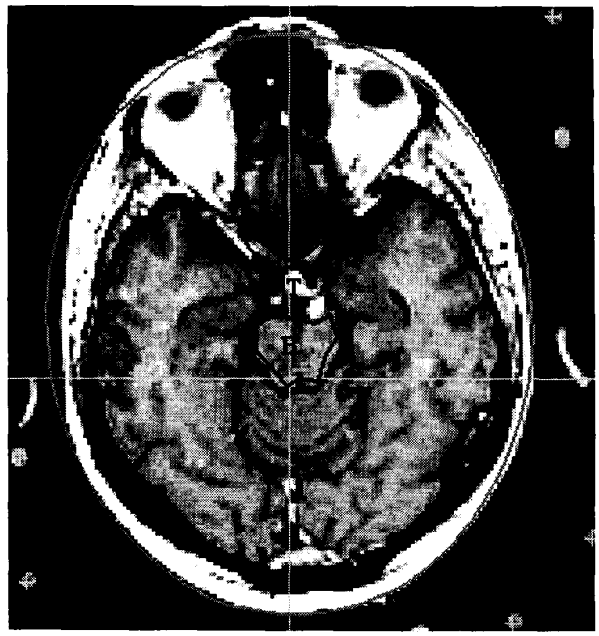

Fig. 7. Axial cross section of the brain in Case 2.

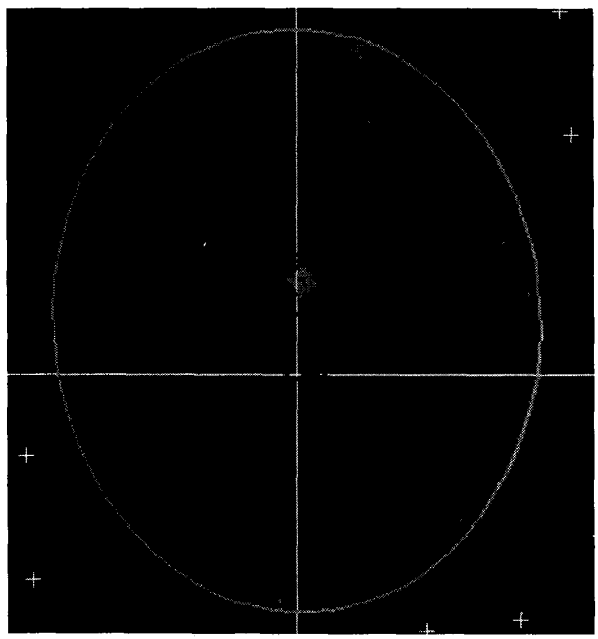

Fig. 8. Energy deposition for the manually planned treatment (Case 2).

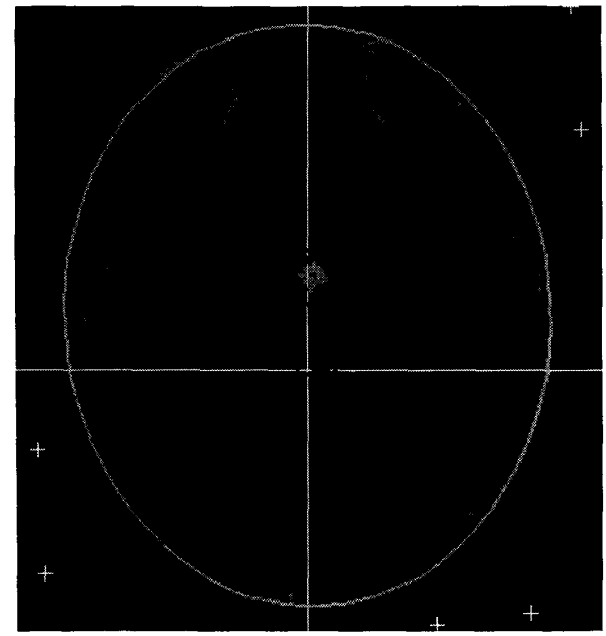

Fig. 9. Energy deposition for the automatically planned treatment (Case 2).

TABLE II
COMPARISON OF ENERGY DOSES IN CASE 2

	manually planned motion		computed motion	
OptNerve.3	27.8	1.4	0.0	0.0
OptNerve.3	173.3	8.7	24.3	1.2
OptNerve.3	159.8	8.0	14.5	0.7
OptNerve.3	46.3	2.3	0.0	0.0
OptNerve.3	57.4	2.9	0.4	0.0
OptNerve.3	35.9	1.8	0.0	0.0
OptNerve.3	140.9	7.0	4.1	0.2
OptNerve.3	199.0	9.9	29.1	1.5
BrStem.3	146.7	7.3	3.3	0.2
BrStem.3	200.5	10.0	7.9	0.4
BrStem.3	70.0	3.5	0.5	0.0
BrStem.3	24.8	1.2	0.0	0.0
BrStem.3	21.7	1.1	0.0	0.0
BrStem.3	17.8	0.9	0.0	0.0
BrStem.3	19.4	1.0	0.0	0.0
BrStem.3	17.9	0.9	0.0	0.0
BrStem.3	24.0	1.2	0.0	0.0
BrStem.3	31.1	1.6	0.0	0.0
BrStem.3	116.0	5.8	8.1	0.4
BrStem.3	104.0	5.2	0.6	0.0
Chiasm.3	322.1	16.1	229.8	11.5
Chiasm.3	404.3	20.2	219.0	11.0
Chiasm.3	364.9	18.2	248.3	12.4
Chiasm.3	135.3	6.8	6.1	0.3
Chiasm.3	174.0	8.7	23.5	1.2
	(a)	(b)	(c)	(d)

consist of four connected arcs in different planes. The tumor was approximated by a single sphere.

Figs. 8 and 9 show energy distribution computed by the dosimetry program in the cross section shown in Fig. 7 for the manually and the automatically planned treatments, respectively. Table II compares dose values at the vertices of the critical regions.

VIII. CONCLUSION

This paper describes a planner developed to help a surgeon generate satisfactory paths for a radiation beam used in radiosurgery. Using geometric techniques, this planner avoids irradiating critical regions of the brain. Experiments on 11 cases indicate that it reduces the path plan-

ning time involved in radiosurgery and improves energy deposition.

The main obstacle to clinical use is insufficient integration of the planner with other software components and its lack of user-friendly interface. Actually, the work presented in this paper is a first step aimed at demonstrating the usefulness of a computer-based planner in radiosurgery. We will soon replace our current LINAC system by a more versatile one using a general 6-degrees-of-freedom gantry. We are currently developing an integrated software package for this new system, which will include medical imagery, treatment planning, and dosimetry simulation.

We envision that significant future progress can be achieved along the following two directions.

- For some locations of a tumor (relative to critical regions), the constraints of our LINAC system seriously reduce the quality of the radiosurgery treatment. Better treatment could be achieved by using a system allowing arcs in both vertical and nonvertical planes. Such a system would make manual planning harder, but this difficulty can be eliminated by an automatic planner. Automatic planning might motivate the development of even more flexible radiosurgical systems.
- In the longer term, faster and more reliable image interpretation techniques should make it possible to directly connect image acquisition to beam control. This could make it possible to eliminate the painful stereotaxic frame attached to the patient's head. It could also allow the application of radiosurgery to the destruction of tumors in parts of the human body that are more difficult to localize in space, e.g., liver and pancreas [11].

Our current research program is articulated along these two directions. We are also investigating techniques for automatically extracting a set of target volumes (e.g., balls, ellipses) from a given tumor, a problem that we have overlooked so far.

Stereotaxic radiosurgery of brain tumors is one instance of so-called "bloodless surgery," for which there is markedly growing interest. We expect that computer-based motion planning techniques such as those described above, together with image interpretation techniques, will facilitate further development of this safer, less painful, and more cost effective type of surgery.

ACKNOWLEDGMENT

The authors thank Rick Cox, Bill Haneman, Paul Hemler, Todd Koumrian, and David Martin from the Stanford Medical Center for making their radiosurgical dosimetry program available to them and discussing various aspects of treatment planning.

REFERENCES

[1] N. H. Barth, "An inverse problem in radiation therapy," *Int. J. Radiat. Oncol. Biol. Phys.*, vol. 18, pp. 425–431, 1990.

[2] M. Bernstein and P. H. Gutin, "Interstitial irradiation of brain tumors: A review," *Neurosurgery*, vol. 9, pp. 741–750, 1981.

[3] O. O. Betti, *et al.*, "Stereotactic radiosurgery with the linear accelerator: Treatment of arteriovenous malformations," *Neurosurgery*, vol. 24, no. 3, pp. 311–321, 1989.

[4] A. Brahme, J. Roos, and I. Lax, "Solution of an integral equation encountered in rotation therapy," *Phys. Med. Biol.*, vol. 27, pp. 1221–1229, 1982.

[5] A. Brahme, "Optimization of stationary and moving beam radiation therapy techniques," *Radiother. Oncol.*, vol. 12, pp. 127–140, 1988.

[6] I. Cohen, L. Cohen, and N. Ayache, "Using deformable surfaces to segment 3D images and infer differential structures," in *Lecture Notes in Computer Science 558*, Sandini, Ed. New York: Springer-Verlag, 1992, pp. 648–652.

[7] A. Cormack, "A problem in rotation therapy with X-rays," *Int. J. Radiat. Oncol. Biol. Phys.*, vol. 13, pp. 623–630, 1987.

[8] A. Cormack and R. Cormack, "A problem in rotation therapy with X-rays. II: Dose distributions with an axis of symmetry," *Int. J. Radiat. Oncol. Biol. Phys.*, vol. 13, pp. 1921–1925, 1987.

[9] H. Edelsbrunner and L. Guibas, "Topologically sweeping an arrangement," *J. Comput. Syst. Sci.*, vol. 38, pp. 165–194, 1989.

[10] L. Guibas and R. Seidel, "Computing convolution by reciprocal search," in *Proc. ACM Symp. Computat. Geometry*, Yorktown Heights, NY, 1986, pp. 90–99.

[11] B. Guthrie and J. Adler, "Frameless stereotaxy: Computer interactive neurosurgery," *Perspectives Neurolog. Surg.*, vol. 2, no. 1, pp. 1–22, 1991.

[12] G. H. Hartmann, "Cerebral radiation surgery using moving field irradiation at a linear accelerator facility," *Int. J. Radiat. Oncol. Biol. Phys.*, vol. 11, pp. 1185–1192, 1985.

[13] H. M. Kooy and N. H. Barth, "The verification of an inverse problem in radiation therapy using Monte Carlo simulations," *Int. J. Radiat. Oncol. Biol. Phys.*, vol. 18, pp. 433–439, 1990.

[14] B. Larsson, *et al.*, "The high energy proton beam as a neurosurgical tool," *Nature*, vol. 182, pp. 1222–1223, 1958.

[15] J.-C. Latombe, *Robot Motion Planning*. Boston, MA: Kluwer, 1991.

[16] S. Lavallée, *et al.*, "Image guided operating robot: A clinical application in stereotactic neurosurgery," in *Proc. IEEE Conf. Robotics Automat.*, Nice, France, 1992, pp. 618–624.

[17] F. Leitner and P. Cinquin, "Dynamic segmentation: Detecting complex topology 3D objects," in *Proc. IEEE Int. Conf. Eng. Med. Biol. Soc.*, Orlando, FL, 1991, pp. 295–296.

[18] L. Leksell, "Cerebral radiosurgery. I: Gamma thalamotony in two cases of intractable pain," *Acta Chir. Scand.*, vol. 13, pp. 585–595, 1968.

[19] T. Lozano-Pérez, "Spatial planning: A configuration space approach," *IEEE Trans. Comput.*, vol. C-32, pp. 108–120, Feb. 1983.

[20] W. Lutz, K. R. Winston, and N. Maleki, "A system for stereotactic radiosurgery with a linear accelerator," *Int. J. Radiat. Oncol. Biol. Phys.*, vol. 14, pp. 373–381, 1988.

[21] H. A. Paul, *et al.*, "A surgical robot for total hip replacement surgery," in *Proc. IEEE Conf. Robotics Automat.*, Nice, France, 1992, pp. 606–611.

[22] B. Pike, E. B. Podgorsak, and T. M. Peters, "Dose distributions in dynamic stereotactic radiosurgery," *Med. Phys.*, vol. 14, no. 5, 1987.

[23] E. B. Podgorsak, *et al.*, "Dynamic stereotactic radiosurgery," *Int. J. Radiat. Oncol. Biol. Phys.*, vol. 14, pp. 115–126, 1988.

[24] E. Welzl, "Smallest enclosing disks," Tech. Rep. B 91-09, Institut für Informatik, FU Berlin, 1991.

[25] K. R. Winston and W. Lutz, "Linear accelerator as a neurological tool for stereotactic radiosurgery," *Neurosurgery*, vol. 22, no. 3, pp. 454–464, 1988.

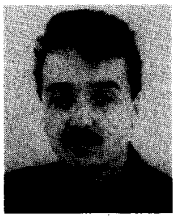

Achim Schweikard received the M.S. degree in mathematics and the Ph.D. degree in computer science in 1985 (Hamburg) and 1989 (Berlin), respectively.

In 1989, he became a visiting scholar at the Robotics Laboratory, Department of Computer Science, Stanford University. In 1992 he received the *venia legendi*. He is currently a Research Associate in the Department of Neurosurgery at Stanford University Medical Center. His areas of research interest include computer algebra, geometric algorithms, and assembly planning.

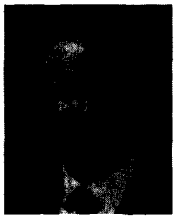

John R. Adler received the A.B. degree in biochemistry from Harvard University, Cambridge, MA, and the M.D. degree from Harvard Medical School, Boston, MA. He performed his residency at the Harvard Medical School Longwood Area Neurosurgical training program.

He is presently an Assistant Professor of Neurologic Surgery and Director of Computerized Stereotaxy at the Stanford University Medical Center, Stanford, CA.

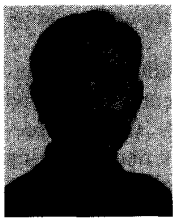

Jean-Claude Latombe received the B.S. and M.S. degrees in electrical engineering and the Ph.D. degree in computer science from the National Polytechnic Institute of Grenoble, in 1969, 1972, and 1977, respectively.

He is currently a Professor of Computer Science at Stanford University, where he is also the Director of the Computer Science Robotics Laboratory. From 1980 to 1984, he was a faculty member at Ecole Nationale Superieure d'Informatique et de Mathematiques Appliquees de Grenoble (ENSIMAG). From 1984 to 1987, he was the executive president of Industry and Technology for Machine Intelligence (ITMI), a company that he cofounded in 1982 for commercializing robot systems and expert systems. His current research interests lie mainly in geometric computing and its applications to automated assembly, mobile robot navigation, design, and computer-assisted surgery.